# A Differential Voltage-Based Wide-Area Backup Protection Scheme for Transmission Network

Shalini and Subhransu Ranjan Samantaray, *Senior Member, IEEE*

***Abstract*—This article proposes a differential voltage-based scheme to identify the faulted line in the transmission system. Initially, the placement of phasor measurement unit (PMU) is carried out. Based on the PMU placement, three subnetwork types are evaluated. Further, a differential voltage-based algorithm is applied to each subnetwork in a system. The tripping decisions for each dependent subnetwork are carried out in steps by providing separate timer settings for them. The load encroachment and fault conditions for a particular case is distinguished by applying modified distance relaying and sequence component-based algorithms to the proposed differential voltage-based scheme. Extensive tests are carried out for several fault and stressed conditions on a New England 39-bus system on MATLAB/Simulink platform. The proposed scheme is also validated for different test cases on a modified WSCC 9-bus system on real-time digital simulator platform for assessing its ability to perform in real time.**

***Index Terms*—Faulted line identification (FLI), phasor measurement unit (PMU) placement, stressed condition, synchrophasor, wide-area backup protection, wide-area measurement (WAM).**

## I. Introduction

### A. Literature Review

With an increase in power demand, the power system is operating closer to its security limits. Due to this, it is susceptible to various power system stressed conditions, such as load encroachment, voltage stressed conditions, and power swing. Conventional relaying schemes may face challenges to discriminate the stressed conditions from the faulted ones [1], [2] and failure may lead to catastrophic blackout situations [3], [4]. Wide-area measurement (WAM)-based protection systems have gained significant momentum in the present scenario due to the development of fast communication and signal processing techniques [5], [6]. Phasor measurement unit (PMU) provides synchronized phasor information for instantaneous ac voltage and current with common time reference provided by GPS signal with an accuracy of 1 $\mu$s.

Several protection schemes focusing on the usage of PMUs for faulted line identification (FLI) have been proposed in the literature. Faulted bus is identified using bus voltage information and the faulted line connected to the faulted bus is found using positive sequence current angle [7]. An adaptive wide-area backup protection (WABP) algorithm finds the faulted backup protection zones using the sum of positive and zero sequence current components [8]. Linear least square scheme is then utilized to find the faulted line using current and voltage phasors in the faulted bus protection zone (BPZ). The above-mentioned schemes have not addressed stressed conditions. A scheme based on bus voltage information for faulted bus identification and cosine of phase-angle difference between current and voltage for FLI is proposed in [9]. However, for fault near strong sources and high-resistance fault cases, the voltage deviation is quite low and comparable with voltage instability situations. Another scheme identifies the faulted line by calculating the ratio of actual bus fault component voltage and estimated voltage from phasor derived from connected PMU bus [10]. In [11], a global comparison of apparent impedances calculated at all the buses using phasors derived from cRIO controller acting as PMUs is carried out. A third zone operation of distance relay is confirmed as the primary relays adjacent to it lies within their zone-1 or zone-2 reach. A scheme based on composite impedance to find the faulty branch is proposed in [12], which is calculated using single end voltage and differential current information. Algorithms for FLI based on differential impedance, differential current, and phase angle of positive sequence integrated impedance (PAPSII) derived using voltage and current phasors at line ends are proposed in [13]–[15], respectively. In [16], two classifiers utilizing PMU information are applied to segregate power swing and voltage instability conditions from fault. However, it requires the generation of large training and testing patterns to perform its task. Schemes [5], [7]–[14] require PMU information from all the buses connecting lines. A synchrophasor-assisted scheme is proposed in [17], where decision tree-based approach is used for state assessment using PMUs at the generator and boundary buses. The FLI is then carried out using the direction of active power flow from the terminals of the lines. In [18], center of reactive power derived from PMU information at generator buses is used to distinguish fault from stressed condition. Further, for FLI, direction of reactive power flow using PMU information from both ends of the line is utilized. Both these schemes require lesser PMU information at the initial stage, thus reducing the phasor data concentrator (PDC) congestion. However, FLI for both the cases require PMU placement at all the buses connecting lines. In [19], voltage phasor information derived at the non-PMU buses using adjacent PMU buses is utilized to identify the faulted bus.

Manuscript received June 23, 2020; revised September 30, 2020 and December 14, 2020; accepted January 19, 2021. Date of publication February 18, 2021; date of current version March 24, 2022. *(Corresponding author: Subhransu Ranjan Samantaray.)*

The authors are with the School of Electrical Sciences, Indian Institute of Technology, Bhubaneswar 752050, India (e-mail: sh16@iitbbs.ac.in; srs@iitbbs.ac.in).

Digital Object Identifier 10.1109/JSYST.2021.3053623

Further, the faulted line is found out by fault location calculation. However, more than half of the system buses are equipped with PMUs. In [20], the voltage at non-PMU buses is calculated from at least two PMU buses connected to it. The percentage voltage deviation is used to find the faulted bus and the current angle difference at the lines connected to the faulted bus is used to find the faulted line. However, the current angle difference-based scheme has a tendency to fail for fault near non-PMU buses. Hence, the scheme shifts to find the faulted line using voltage calculated at non-PMU buses from connected PMU buses which may maloperate for fault near PMU buses. Hence, this scheme requires three subroutines and a huge data sharing from all the buses in the system. A method applying Kirchoff's current law (KCL) at non-PMU bus from phasors derived from PMU buses is proposed in [21].Though the PMU requirement is reduced, it assumes the calculation of phasors at non-PMU bus considering prefault load values. This may fail to distinguish some fault conditions from voltage stressed situations. In [22], an index based on voltage information is derived for identifying the faulted line with unavailable synchrophasor information at critical buses due to communication failure. However, initially the PMUs are placed at all the buses. Moreover, it requires a non-PMU bus connected to at least three PMU buses at all times. In [23], a wide-area protection scheme is devised using a gain in momentum of generators to find the vulnerable protection zone. Further, the faulted bus and faulted line are identified using positive sequence bus-voltage and reactive power of the lines connected to the faulted bus. For this, the PMUs are placed at all the generator buses as well as the buses corresponding to vulnerable buses which needs zone-3 replacement.

### B. Motivation and Incitement

Owing to the drawbacks and gaps from the literature mentioned above, the motivations leading to the development of the proposed scheme are summarized as follows.

1) The issues related to relay maloperation using traditional distance relays can be addressed using WAMs-based scheme. Some of the existing schemes dealing with FLI are not validated for power system stressed conditions, which may lead to unnecessary relay tripping during stressed conditions.
2) Majority of the schemes for FLI require PMU placement at large number of buses. However, due to economic constraints it is not feasible to install PMUs at many buses.
3) Information sharing among large number of buses requires huge communication infrastructure and congestion at the PDC end.
4) Some schemes may lose its dependability for fault near strong sources and high-resistance faults.

### C. Contribution and Article Organization

To alleviate the aforementioned problems, a new backup protection scheme is proposed in this article which addresses the following issues.

1) The proposed scheme aims at providing backup protection for the transmission network, which has the ability to distinguish fault from different stressed conditions such as line outage, generator outage, load encroachment, and voltage stressed conditions.
2) It utilizes limited synchrophasor information for FLI.
3) A differential voltage-based method is proposed to deal with FLI for different subnetwork types considered after the PMU placement.

The article is organized as follows. Section II gives a detailed explanation of the proposed scheme. Section III outlines the performance evaluation of the proposed scheme for various power system faults and stressed conditions on a 39-bus and 9-bus system, including real-time digital simulator (RTDS) tests. Section IV compares the proposed scheme with existing schemes and Section V concludes this article.

## II. Proposed Method

### A. PMU Placement

A PMU installed at any bus can measure its voltage phasor and the current phasors of all the lines connected to it. Using the phasor data available at a PMU bus and the line parameters of the connected line, the phasor at the adjacent bus can be derived [24]. The following rules for PMU placement are incorporated for the proposed scheme.

1) The line ends of all the generator or transformer bus are equipped with PMUs.
2) The radial buses connected to lines are equipped with PMUs.
3) For the remaining buses connecting lines, a bus connected to "*N*" lines should either be equipped with PMU or connected to $(N-1-Z_n)$ PMUs. Hence, the PMU placement is formulated by solving the objective function as

$$\text{Minimize} \sum_{i \epsilon B} x_i \text{ subject to}$$
$$f_i \geq \text{Max}(0, N_i - 1 - Z_{in}), \forall i \epsilon B \text{ and } x_i = 1 \forall i \epsilon G, R \tag{1}$$

where, $N_i$ is the number of lines connected to bus-i and $Z_{in}$ is the number of zero injection bus/es connected to *i* which is connected to all the PMU buses through lines except one

$$f_i = \sum_{\substack{j \epsilon B \\ j \neq i}} \text{Max}(0, N_i - 1 - Z_{in}) a_{ii} x_i + a_{ij} x_j. \tag{2}$$

$a_{ij}$ is the branch connectivity between i and j such that

$$a_{ij} = \begin{cases} 1 \text{ if } i = j \text{ or } i \text{ and } j \text{ are connected} \\ 0 \text{ otherwise} \end{cases} \tag{3}$$

$$x_i = \begin{cases} 1 \text{ if } i \text{ is equipped with } PMU \\ 0 \text{ otherwise.} \end{cases} \tag{4}$$

Hence, the PMU placement problem can be solved using integer linear programming (ILP).

4) After PMU placement using the above rules, an additional criteria is checked, where a maximum of two adjacent load

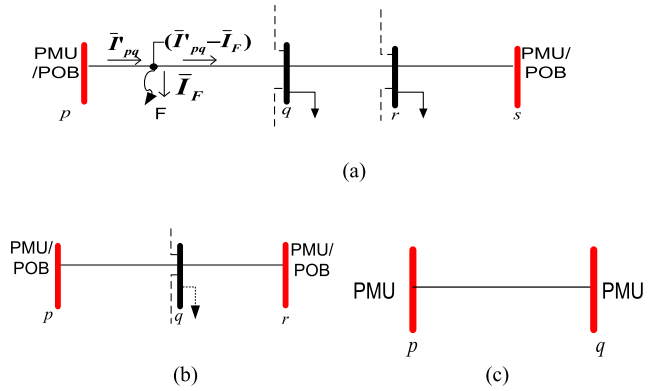


Fig. 1. Studied subnetwork types in a transmission network. (a) SNT-1. (b) SNT-2. (c) SNT-3.

buses should be non-PMU buses. PMU should be added accordingly to meet this requirement.

### B. FLI Method for Different Subnetwork Types (SNTs)

Three SNTs are possible after PMU placement.

The non-PMU zero injection buses which are observed through all the connected PMU buses except one is termed here as PMU observable buses (POB).

1) *Subnetwork Type 1 (SNT-1):* It consists of two non-PMU buses connected to the PMU buses or POB on either sides, as shown in Fig. 1(a). Consider the line sections p-q-r-s, with PMU/POB buses p and s. The voltages at non-PMU buses q and r, are achieved using phasor information at p and s, respectively

$$\bar{V}_q^p = \bar{V}_p - \bar{I}_{pq}\bar{Z}_{pq} + \bar{V}_p\frac{\bar{Y}_{pp,q}}{2}\bar{Z}_{pq} \tag{5}$$

$$\bar{V}_r^s = \bar{V}_s - \bar{I}_{sr}\bar{Z}_{sr} + \bar{V}_s\frac{\bar{Y}_{ss,r}}{2}\bar{Z}_{sr}. \tag{6}$$

The line current from bus-r to bus-q is given as

$$\bar{I}_{rq} = -\bar{I}_{rs} - \bar{I}_{Lr} \tag{7}$$

where

$$\bar{I}_{rs} = \frac{\bar{V}_r^s - \bar{V}_s}{\bar{Z}_{sr}} + \bar{V}_r^s\frac{\bar{Y}_{rr,s}}{2}\bar{Z}_{sr} \tag{8}$$

and

$$\bar{I}_{Lr} = \frac{(P_{Lr} - jQ_{Lr})}{(\bar{V}_r^s)^*} \tag{9}$$

are the line currents from bus-r to bus-s and load current at bus-r, respectively

$$\text{Real}\ (\bar{I}_{Lr}) = |I_{Lr}|\cos\phi_{Lr} = \frac{P_{Lr}\cos\delta_r^s}{|V_r^s|} + \frac{Q_{Lr}\sin\delta_r^s}{|V_r^s|} \tag{10}$$

$$\text{Imag}\ (\bar{I}_{Lr}) = |I_{Lr}|\sin\phi_{Lr} = \frac{P_{Lr}\sin\delta_r^s}{|V_r^s|} - \frac{Q_{Lr}\cos\delta_r^s}{|V_r^s|}. \tag{11}$$

Now, the voltages at buses q and r measured through buses s and p are given as

$$\bar{V}_q^s = \bar{V}_r^s - \bar{I}_{rq}\bar{Z}_{rq} + \bar{V}_r^s\frac{\bar{Y}_{rr,q}}{2}\bar{Z}_{rq} \tag{12}$$

$$\bar{V}_r^p = \bar{V}_q^p - \bar{I}_{qr}\bar{Z}_{rq} + \bar{V}_q^p\frac{\bar{Y}_{qq,r}}{2}\bar{Z}_{rq}. \tag{13}$$

For no disturbance inside section p-q-r-s, $\bar{V}_q^p - \bar{V}_q^s \approx 0$ and $\bar{V}_r^s - \bar{V}_r^p \approx 0$ .However, for a fault at any of the lines or load increase at buses q as well as r, $\bar{V}_q^p - \bar{V}_q^s \neq 0$ and $\bar{V}_r^s - \bar{V}_r^p \neq 0$.

The differential voltage factor (DVF) at the monitored buses "q" and "r" are defined as

$$\begin{aligned}
\text{DVF}_{\text{q}}^{\text{p,s}} &= \cos(\delta_r^s) * Re\left(\bar{V}_q^p - \bar{V}_q^s\right) + \sin(\delta_r^s) * Im\left(\bar{V}_q^p - \bar{V}_q^s\right)\\
\text{DVF}_{\text{q1}}^{\text{p,s}} &= \cos(\delta_p) * Re\left(\bar{V}_q^p - \bar{V}_q^s\right) + \sin(\delta_p) * Im\left(\bar{V}_q^p - \bar{V}_q^s\right)\\
\text{DVF}_{\text{r}}^{\text{s,p}} &= \cos\left(\delta_q^p\right) * Re\left(\bar{V}_r^s - \bar{V}_r^p\right) + \sin\left(\delta_q^p\right) * Im\left(\bar{V}_r^s - \bar{V}_r^p\right)\\
\text{DVF}_{\text{r1}}^{\text{s,p}} &= \cos(\delta_s) * Re\left(\bar{V}_r^s - \bar{V}_r^p\right) + \sin(\delta_s) * Im\left(\bar{V}_r^s - \bar{V}_r^p\right).
\end{aligned} \tag{14}$$

For an increase in load at bus-r, $\text{DVF}_{\text{r}}^{\text{s,p}} \approx 0$ .The correct voltage at bus-q is defined using (5). Whereas, the voltage phasor derived using (12) is incorrect. Let $\bar{V}_q^{s'}$ and $\bar{I}'_{rq}$ be the correct voltage and current phasors for load increase at bus-r

$$\bar{V}_q^{s'} = \bar{V}_r^s - \bar{I}'_{rq}\bar{Z}_{rq} + \bar{V}_r^s\frac{\bar{Y}_{rr,q}}{2}\bar{Z}_{rq}. \tag{15}$$

Using (5)–(14) and $\bar{V}_q^{s'} = \bar{V}_q^p$ , $\text{DVF}_{\text{q}}^{\text{p,s}}$ is obtained as

$$\begin{aligned}
\text{DVF}_{\text{q}}^{\text{p,s}} = {} & \frac{Z_{rq}\cos(\theta_{rq})}{|V_r^s|}\left(P'_{Lr} - P_{Lr}\right)\\
& + \frac{Z_{rq}\sin(\theta_{rq})}{|V_r^s|}\left(Q'_{Lr} - Q_{Lr}\right)
\end{aligned} \tag{16}$$

where $P'_{Lr}$ and $P_{Lr}$ are the actual load value and predisturbance load value at bus-r, respectively. Since $P'_{Lr} > P_{Lr}$ and $Q'_{Lr} > Q_{Lr}$ for active and reactive load increase, an increase in active power and/or reactive power demand at bus-r gives a positive value for $\text{DVF}_{\text{q}}^{\text{p,s}}$. Similarly, for a load increase at bus-q, $\text{DVF}_{\text{q}}^{\text{p,s}} \approx 0$ and $\text{DVF}_{\text{r}}^{\text{s,p}}$ is positive.

Let us consider a fault on line p-q. For this situation, the voltage at bus-q derived from (12) is correct and that from (5) is incorrect. Let $\bar{V}_q^{p'}$ be the correct voltage such that $\bar{V}_q^{p'} = \bar{V}_q^s$ . Assume $\bar{I}'_{pq} = \bar{I}_{pq} - \bar{V}_p\frac{Y_{pp,q}}{2}$.

For a fault occurring at a distance "*D*" from bus-p

$$\begin{aligned}
\bar{V}_F &= \bar{V}_p - \bar{I}'_{pq}\bar{Z}_{pq}D\\
\bar{V}_q^{p'} &= \bar{V}_F - \left(\bar{I}'_{pq} - \bar{I}_F\right)\bar{Z}_{pq}(1-D)\\
\bar{V}_q^{p'} &= \bar{V}_p - \bar{I}'_{pq}\bar{Z}_{pq}D - \left(\bar{I}'_{pq} - \bar{I}_F\right)\bar{Z}_{pq}(1-D).
\end{aligned} \tag{17}$$

The DVF at bus-q using phasor information from buses p and s for fault at line p-q gives

$$\begin{aligned}
\text{DVF}_{\text{q}}^{\text{p,s}} &= -I_F Z_{pq}(1-D)\cos(\phi_F + \theta_{pq} - \delta_r^s)\\
\text{DVF}_{\text{q1}}^{\text{p,s}} &= -I_F Z_{pq}(1-D)\cos(\phi_F + \theta_{pq} - \delta_p).
\end{aligned} \tag{18}$$

TABLE I
SIGN OF THE DVF INDEX FOR FAULT AND LOAD INCREASE

| Disturbance cases | $DVF_q$ | $DVF_r$ | $DVF_{q1}$ | $DVF_{r1}$ |
|---|---|---|---|---|
| Fault at line p-q | (-) | - | (-) | (+) |
| Fault at line r-s | - | (-) | (+) | (-) |
| Fault at line q-r | (+) | (+) | (+) | (+) |
| Load increase at bus-q | 0 | (+) | - | - |
| Load increase at bus-r | (+) | 0 | - | - |
| Load increase at bus-q and r | (+) | (+) | - | - |

Normally, the impedance angle ($\theta_{pq}$) lies between 70°–88° due to the presence of high inductive element with respect to resistive element. Since the fault impedance at the fault point is predominantly resistive in nature, the phase angle between voltage and current at the fault point is almost equal to zero. Hence, voltage and current angle ($\phi_F$) at the fault point are almost equal. For a fault at line p-q, the power flow is from bus-p and bus-r to the fault point. This implies that the angle $(\phi_F - \delta_p)$ and $(\phi_F - \delta_r^s)$ are negative. The cosine term in (18) is positive for

$$-178^\circ < (\phi_F - \delta_r^s) < 0^\circ (\text{for } \theta_{pq} = 88^\circ). \tag{19}$$

Hence, $\mathrm{DVF_q^{p,s}}$ and $\mathrm{DVF_{q1}^{p,s}}$ are negative for a fault on line p-q. Now, the DVF value at bus-r is calculated for the same condition. Let the correct voltage at bus-r calculated from bus-p be given as $\bar{V}_r^{p'} = \bar{V}_r^s$

$$\left(\bar{V}_r^{p'} - \bar{V}_r^p\right) = \left(\bar{V}_q^s - \bar{V}_q^p\right) + \left(\bar{V}_q^s - \bar{V}_q^p\right)\left(\frac{Y_{qq,r}}{2}\right)\bar{Z}_{qr} - \left(\bar{I}_{qr}^s - \bar{I}_{qr}^p\right)\bar{Z}_{qr} \tag{20}$$

where

$$\left(\bar{I}_{qr}^s - \bar{I}_{qr}^p\right) = -\bar{I}_F - \left(\bar{V}_q^s - \bar{V}_q^p\right)\left(\frac{Y_{qq,p}}{2}\right). \tag{21}$$

Since, $\mathrm{DVF_r^{s,p}}$ depends on $\delta_q^p$, which is incorrect for the present scenario, its value is incorrect. Hence, $\mathrm{DVF_{r1}^{s,p}}$ is also calculated

$$\begin{aligned}\mathrm{DVF_{r1}^{s,p}} = {} & I_F Z_{pq}(1-D)\cos(\phi_F + \theta_{pq} - \delta_s) \\ & + I_F Z_{qr}\cos(\phi_F + \theta_{qr} - \delta_s) \\ & + I_F Z_{qr} Z_{pq}(1-D)\left(\frac{Y_{qq,p}}{2} + \frac{Y_{qq,r}}{2}\right) \\ & \times \cos(\phi_F + \theta_{qr} + \theta_{pq} + 90^\circ - \delta_s).\end{aligned} \tag{22}$$

Based on the theory stated for (18), the first and second terms of $\mathrm{DVF_{r1}^{s,p}}$ in (22) are positive. The cosine term inside the third term may be positive or negative. However, the admittance term nullifies the third term with respect to the first and second term. Hence, the magnitude part of these terms will lead to a positive value for (22).

Table I states the behavior of the index for different disturbance situations. Hence, at the monitored subnetwork, $\mathrm{DVF}_q^{p,s}$, $\mathrm{DVF}_{q1}^{p,s}$, $\mathrm{DVF}_r^{s,p}$, and $\mathrm{DVF}_{r1}^{s,p}$ are observed to identify the faulted line. Thus, for a faulted line p-q

$$\mathrm{DVF}_q^{p,s} \langle -Th \;\&\; (\mathrm{DVF}_r^{s,p}\rangle 0 \; OR \; \mathrm{DVF}_{r1}^{s,p} > 0). \tag{23}$$

Similarly, for a fault at line r-s

$$\mathrm{DVF}_r^{s,p} \langle -Th \;\&\; (\mathrm{DVF}_q^{p,s}\rangle 0 \; OR \; \mathrm{DVF}_{q1}^{p,s} > 0) \tag{24}$$

where $Th$ is the threshold value for fault detection.

From Table I, it is observed that, for fault at lines p-q and r-s, one of the DVF indices crosses the negative threshold. However, it may fail to distinguish between the fault at q-r and load increase at bus-q as well as bus-r, since DVF at q and r for both the cases is positive. To address this issue, an additional modified distance relay (MDR) scheme is applied in which apparent impedance using PMU/POB information from buses p and s are calculated. From bus-p, the network is assumed to be divided into two protection zones such that the first zone is 80% of the line section p-q and the second zone is line p-q and 60% of the line section q-r. Similarly, the zones are divided from bus-s for the line section p-q-r-s. To make the scheme more robust against high-resistance unsymmetrical faults, sequence current component-based scheme is added. It is based on the presence of negative and zero sequence components for unsymmetrical faults and its absence for load increase. Hence, the sum of negative and zero sequence current (SNZC) is obtained from phasor information at buses p and s for lines p-q and s-r. Power system stressed conditions such as load encroachment and voltage stressed conditions mostly affect the third zone of a distance relay. Considering this fact, for a fault on line q-r, the apparent impedance lies within the zone-2 of bus-p and s. Thus, for a fault on line q-r

$$\begin{aligned}&\mathrm{DVF}_q^{p,s} > +Th \;\&\; \mathrm{DVF}_r^{s,p} > +Th \;\& \\ &Z_{\mathrm{app},p} < Z_{Z2,p} \; OR \; Z_{\mathrm{app},s} < Z_{Z2,s} \; OR \\ &\mathrm{SNZC} = \left|I_{p-q}^-\right| + \left|I_{p-q}^0\right| + \left|I_{s-r}^-\right| + \left|I_{s-r}^0\right| > h\end{aligned} \tag{25}$$

where $Z_{\mathrm{app},p}$ and $Z_{\mathrm{app},s}$ are apparent impedances calculated using phasor information from bus-p and s, respectively. $Z_{Z2,p}$ and $Z_{Z2,s}$ are the zone-2 settings from bus-p and s, respectively. $I_{p-q}^-$, $I_{p-q}^0$, $I_{s-r}^-$, and $I_{s-r}^0$ are the negative and zero sequence current components from buses p and s. $h$ is the threshold which is set as 0.1 p.u. based on system analysis for high-resistance fault cases on line q-r.

2) *Subnetwork Type-2 (SNT-2):* This type of network consists of two or more PMU/POB buses connected to a non-PMU bus (zero injection/load bus) as shown in Fig. 1(b). Hence, similar to SNT-1, the DVF for SNT-2 is defined as

$$\begin{aligned}\mathrm{DVF}_q^{p,r} = {} & \cos(\delta_p) * Re\left(\bar{V}_q^p - \bar{V}_q^r\right) \\ & + \sin(\delta_p) * Im\left(\bar{V}_q^p - \bar{V}_q^r\right).\end{aligned} \tag{26}$$

With the similar theory as stated for SNT-1, the index for FLI for a fault on line p-q should verify

$$\mathrm{DVF}_q^{p,r} < -Th. \tag{27}$$

Similarly for a fault on line q-r

$$\mathrm{DVF}_q^{p,r} > +Th. \tag{28}$$

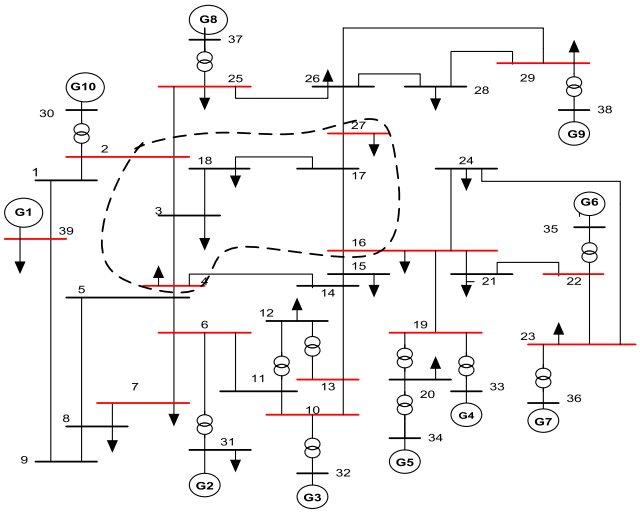


Fig. 2. New England 39-bus system.

2) *Subnetwork Type-3 (SNT-3):* This type of subnetwork consists of two PMU buses connected to each other as shown in Fig. 1(c). The concept discussed in [10] for a two-terminal system with difference in actual bus-voltage at a PMU bus and estimated voltage from connected PMU bus for an internal fault case is utilized here. For this case, the index is derived as

$$\mathrm{DVF}_p^q = \left|\bar{V}_p^p - \bar{V}_p^q\right| \tag{29}$$

where $\bar{V}_p^p$ is the voltage phasor measured at bus-p through its own PMU and $\bar{V}_p^q$ is the voltage phasor measured through PMU at bus-q. For a faulted line p-q

$$\mathrm{DVF}_p^q > Th. \tag{30}$$

The subnetwork consisting of buses for which the DVF can be directly obtained from the connected PMU buses are termed as independent subnetworks. However, the subnetwork for which the index is derived using information from independent subnetwork is termed as dependent subnetwork. To understand this concept, a portion of New-England 39-bus system is studied, as shown in Fig. 2. Subnetworks 2-3-4 and 16-17-27 are independent subnetworks, since phasor information at non-PMU buses 3 and 17 are directly derived from PMU buses 2–4 and 16–27, respectively. However, subnetwork 3-18-17 is a dependent subnetwork, since the phasor information at bus-18 can again be derived using the phasor information at non-PMU buses 3 and 17.

For two or more dependent subnetworks, the fault in one subnetwork may cause the index at the faulty subnetwork as well as the subnetwork connected to it to cross the threshold. This is undesirable, since a protection system is expected to trip a minimum possible line section to maintain proper power flow in the system. The DVF for the independent as well as dependent subnetwork may cross the threshold at the same time or the DVF for the dependent subnetwork may cross the threshold before the connected independent subnetwork. Hence, for a fault at an independent subnetwork, a block command is sent to the decision for connected dependent subnetwork. Thus, a sufficient time delay of 100 ms is allotted for the operation of dependent network to prevent incorrect decision from the DVF calculated for dependent subnetwork. After the PMU placement is carried out as per Section II-A, it should be checked that a maximum of the two subnetworks dependent on the information from the independent subnetwork should be connected. A PMU should be added accordingly, if the number of dependent subnetworks is more than two. The PMU placement for different system is tabulated in Table II. For 39 bus-system, from placement rules, the number of required PMUs are 13 with no PMU at bus-7. For this, the index is first derived at bus-5 through PMU buses 6 and 7 forming an independent SNT-2. The dependent subnetworks comprise of three subnetworks 5-8-9, 39-9-8, and 8-7-6. Hence, a PMU is added at bus-7 to reduce the dependent subnetworks to two. The relay tripping criteria for different fault situation is summarized in Table III. SNT-1 consists of two PMU/POB buses P1 and P2 and two non-PMU buses N1 and N2 to form a line section P1-N1-N2-P2. SNT-2 consists of single non-PMU bus (N) connected to two PMU/POB buses (P1 and P2) and SNT-3 consists of two connected PMU buses (P1 and P2). From (18), it is observed that the faulted line is identified using the sign of the DVF index for SNT-1 and SNT-2. However, to eliminate any possibility of nuisance tripping of the relay due to switching events, measurement or calculation errors, a suitable threshold should be selected. The index magnitude for fault case is mainly dependent on the fault current ($I_{\mathrm{F}}$), fault location ($D$), and line impedance. Hence, the threshold is set by carrying out extensive tests for extreme conditions and observing the index at the monitored faulty bus for far-end, high-resistance fault from PMU bus at the lines having minimum impedances for the subnetworks located far from sources. The index is also observed for nonfaulty buses for a near-end solid three-phase fault for the lines. Based on the observations, the absolute threshold value is selected as 50 V. The flowchart of the proposed scheme is shown in Fig. 3.

TABLE II
PMU PLACEMENT FOR PROPOSED SCHEME

| System Studied | PMU buses – (Number of PMU buses) |
|---|---|
| WSCC 9-bus System | 4,7,9 – (3) |
| New-England 39-bus System | 2,4,6,7,10,13,16,19,,22,23,25,27,29,39 – (14) |
| IEEE 57-bus system | 1,2,3,6,8,9,11,12,15,18,21,24,28,31,35,37, 47,48,50,53,56 (21) |

## III. PERFORMANCE ASSESSMENT OF THE PROPOSED SCHEME

The proposed scheme is evaluated on a New England 10-machine 39-bus system of 60 Hz system frequency [25] using MATLAB/Simulink, as shown in Fig. 2, with PMU placed at buses marked in red. The objective function for PMU placement is solved using ILP in MATLAB toolbox with CPLEX solver. IEEE C37.118-1 compliant P-class PMUs [26], [27] are utilized to extract the phasor information from PMU buses with a phasor

TABLE III
RELAY TRIPPING CONDITION FOR DIFFERENT FAULT SITUATIONS

| Sub-network phasor dependency | Sub-network type | Relaying Condition | Decision | Response time ($T_R$) |
|---|---|---|---|---|
| Fault at independent sub-network | SNT-1 | $DVF_{N1}^{P1,P2} < -Th$ & $DVF_{N2}^{P2,P1} > 0$ OR $DVF_{N2,1}^{P2,P1} > 0$ | Fault detected at line connecting P1-N1 | $T_{PMU}$ [27]= 75 ms (Fixed delay –PDC processing +Transducers+Multiplexing) +25 ms (Delay due to communication medium - Fibre optics) $T_D$ =Fault detection time $T_R = T_{PMU} + T_D$ |
| | SNT-1 | $DVF_{N2}^{P2,P1} < -Th$ & $DVF_{N1}^{P1,P2} > 0$ OR $DVF_{N1,1}^{P1,P2} > 0$ | Fault detected at line connecting P2-N2 | |
| | SNT-1 | $DVF_{N1}^{P1,P2} > +Th$ & $DVF_{N2}^{P2,P1} > +Th$ & $Z_{app,P1} < Z_{Z2,P1}$ OR $Z_{app,P2} < Z_{Z2,P2}$ OR $\lvert I_{P1}^{-} + I_{P1}^{0} + I_{P2}^{-} + I_{P2}^{0} \rvert > h$ | Fault detected at line connecting N1-N2 | |
| | SNT-2 | $DVF_{N}^{P1,P2} < -Th$ | Fault detected at line connecting P1-N | |
| | SNT-2 | $DVF_{N}^{P1,P2} > +Th$ | Fault detected at line connecting P2-N | |
| | SNT-3 | $DVF_{P1,P2} > +Th$ | Fault detected at line connecting P2-P1 | |
| Fault at dependent sub-network | SNT-1 | Same criterion as of independent sub-network Wait time allotted between operation of each dependent sub-network, △T=100 ms | | For 1st dependent sub-network- $T_{PMU}$ +△T For 2nd dependent sub-network- $T_{PMU}$ +2× △T |
| | SNT-1 | | | |
| | SNT-2 | | | |

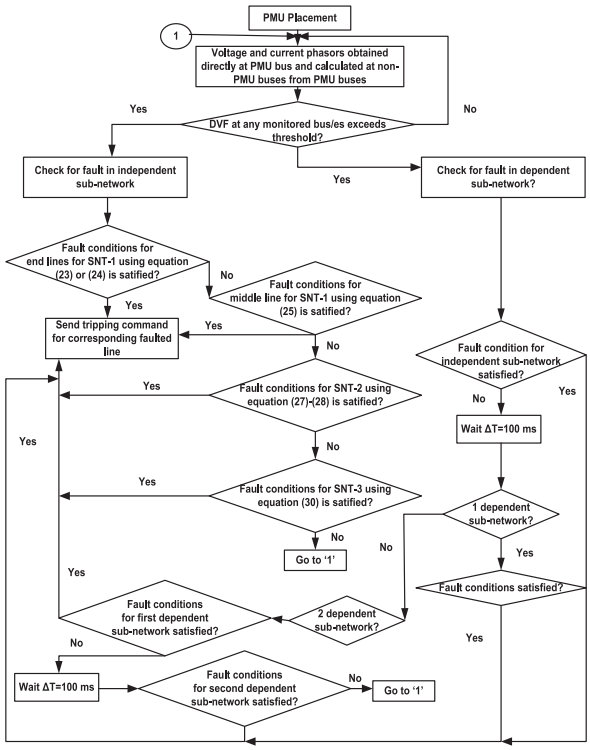


Fig. 3. Flowchart for the proposed scheme.

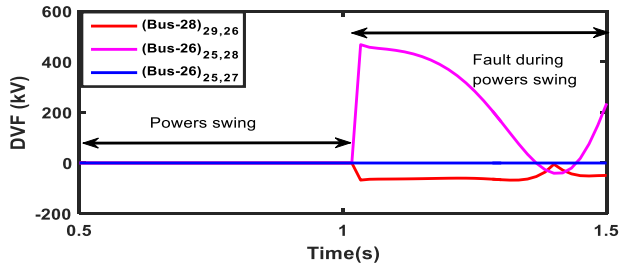


Fig. 4. DVF at 26 and 28 for fault at line 28-29 during power swing at line 28-29.

reporting rate of 60 frames/s [28], [29]. Simulations are carried out on a DELL Core i5-2400 CPU at 3.1 GHz with 8 GB RAM. The index is derived for all the subnetworks to study the performance of the scheme for faulted and system stressed conditions. The results are illustrated for the buses with maximum deviation in the index for the simulated disturbances.

### A. Performance Assessment During Stressed Conditions

Power system stressed conditions mainly include stable power swing, generator outage, load encroachment, and voltage stressed conditions. These may lead to inadvertent relay tripping and thus, endangering the system security.

Power swing results due to sudden disturbances such as line switching, faults, and switching OFF of heavy loads [30]. A fault is created at line 26–29 and subsequently isolated within five cycles by opening the breakers associated to it. This creates a stable power swing situation for line 28-29. The independent subnetwork consists of a non-PMU bus-26 connected to PMU buses 25, 27, and 29. The DVF at bus-26 is first calculated using PMUs at bus-25 and 27. This results in no significant deviation. After a delay of 100 ms, the DVF at bus-26 and bus-28 is observed, which is calculated using phasor information at bus-28 (derived using PMU bus-29) and bus-26 (derived using PMU at bus-25 and 29), respectively. None of the DVF indexes cross the threshold, indicating no fault situation. For a fault on line 28-29 during the power swing, the DVF at bus-26 and bus-28 are found using phasor measurements at bus-25, 27, and 29. At bus-26, the $DVF_{26}^{25,27}$ does not cross the threshold, indicating no fault on the connecting lines. However, from Fig. 4, $DVF_{26}^{25,28}$ is positive and $DVF_{28}^{29,26}$ crosses the negative threshold, confirming a fault on line 28-29.

The effect of generator outage is demonstrated by disconnecting the generator connected to bus-32 at 1 s. The DVF at bus-11 and bus-13 calculated using PMU information at buses 6, 10

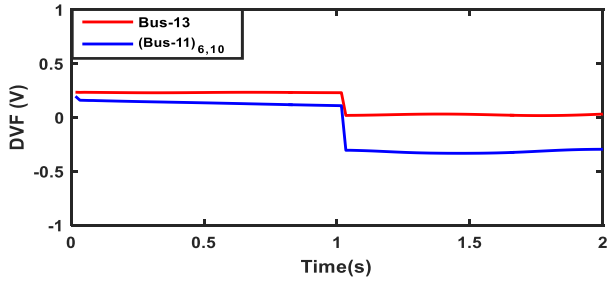


Fig. 5. DVF at 11 and 13 for generator outage at bus-32.

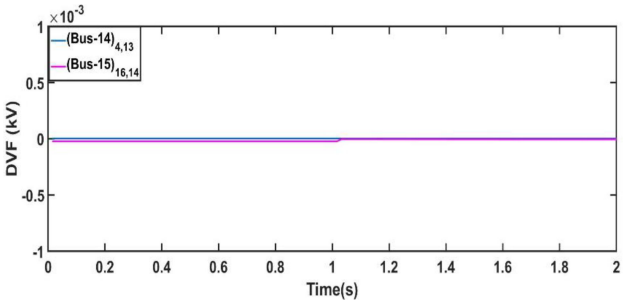


Fig. 6. DVF at 14 and 15 for load increase at bus-15.

and 13, respectively, does not cross the threshold, verifying a no-fault situation, as shown in Fig. 5.

Load encroachment is the result of increase in load at some of the buses so that the impedance trajectory encroaches inside the operating characteristic of distance relay. The load at bus 15 is increased, considering the North American Electric Reliability Council (NERC) criterion for extreme loading condition for zone-3 operation [31]. First, the DVF index at bus-14 obtained through PMU buses 4 and 13 (forming SNT-2) is used to establish a no-fault situation at lines 4–14 and 13-14. Thereafter, the index at bus 15 is observed, which is derived using PMU buses 4–13 and 16 after a wait time of 100 ms. Fig. 6 shows that the index does not cross the threshold, indicating a no-fault situation.

To assess the proposed scheme for voltage stressed situation, reactive power at buses 3, 4, 18, and 27 are increased simultaneously. The DVF at bus-3 using phasors at bus-2 and bus-17 is then observed. Similarly, the DVF at bus 18 obtained using phasors at bus-3 and bus-17 is observed. The results in Fig. 7(a) showing the DVF index at 3 and 18 crossing their thresholds indicates a possibility of either a fault at line 3–18 or a load increase at buses 3 and 18 for SNT-1 2-3-18-17. To verify a fault or no-fault situation, an MDR-based approach is utilized. For this, the impedance at bus-2 and bus-17 for lines 2-3 and 17-18 are calculated. The R-X trajectory at bus-2 and17 shows that it does not enter the zone-2 characteristics of MDR, as shown in Fig. 7(b). The SNZCs derived for lines 2-3 and 17-18, as shown in Fig. 7(c), shows a negligible deflection for this situation. Hence, there is no fault in the network.

The summary of the performance of proposed scheme showing the results for the most affected bus during stressed condition is given in Table IV.

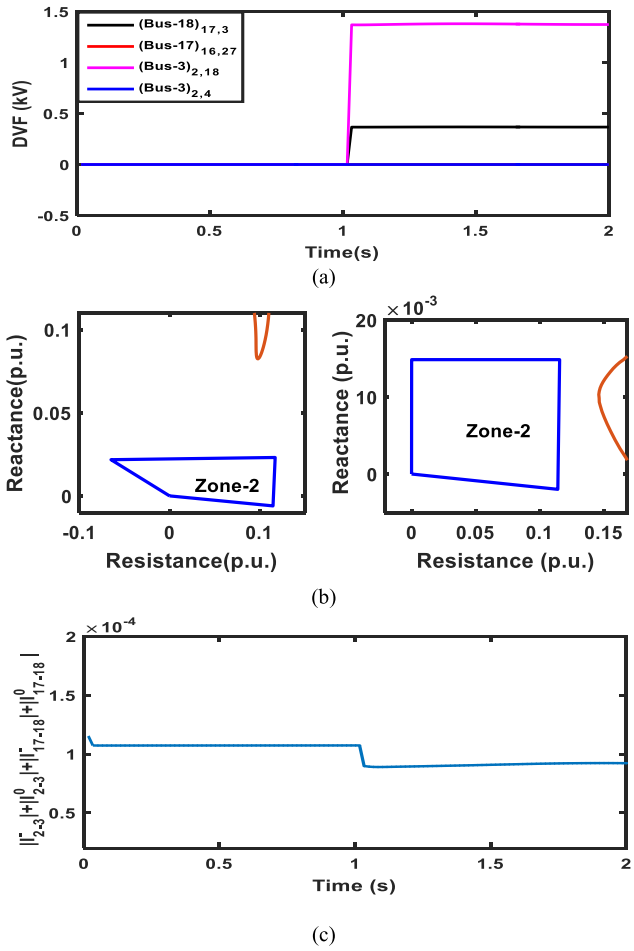


Fig. 7. Voltage stressed condition. (a) DVF at buses 317 and 18. (b) MDR characteristics for bus-2 and 17. (c) SNZC from bus-2 and bus-17.

TABLE IV
DVF INDEX FOR DIFFERENT STRESSED CONDITIONS

| Disturbance situation | Affected bus | DVF(kV) |
|---|---|---|
| Power swing due to line outage at 26-29 | 28 | 0.00022 |
| Generator outage at bus-30 | 25 | -0.00034 |
| Generator outage at bus-32 | 11 | 0.0003 |
| Reactive load increase at bus-18 | 3 | 1.4 |
| Load increase at bus-8 | 9 | 24.840 |

### B. *Performance Assessment for Different Fault Cases*

The proposed scheme is studied for the four fault types (A-G, A-B, AB-G, and ABC) with a fault resistance of 10 Ω for the line 26–28. Fig. 8(a) for AB fault shows a negligible deviation in index at bus-26 using PMUs 25, 27, and 29. It is observed that the index from the dependent subnetwork at bus-26 and 28, after a wait time of 100 ms, crosses their respective positive thresholds. This indicates either a fault at line 26–28 or a load increase at bus-26 and 28. The MDR approach is now considered at bus-25 and 29 for the line section 25-26-28-29 where the relay trajectory crosses their zone-2, as shown in Fig. 8(b), confirming a fault

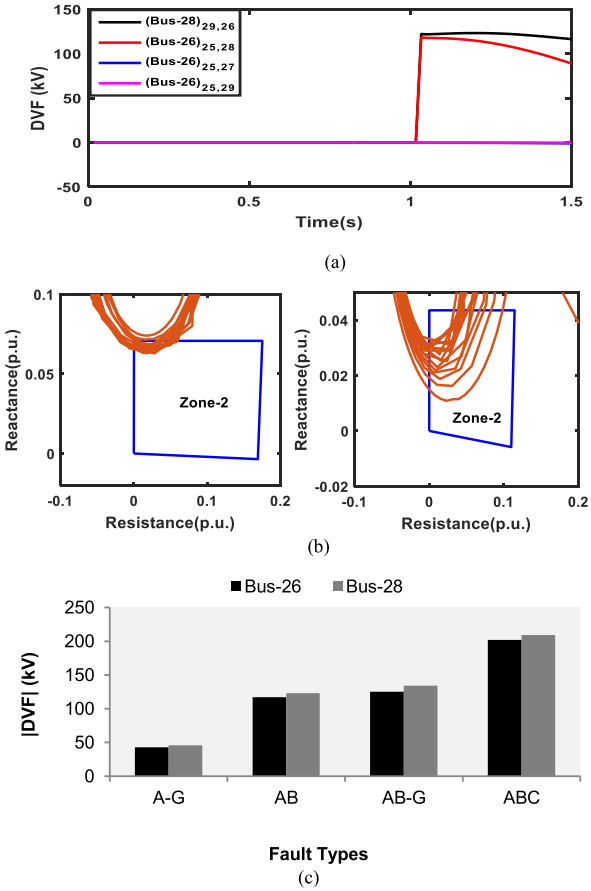


Fig. 8. Fault at line 26–28 with $R_f = 10\,\Omega$ at 1 s. (a) DVF for AB fault. (b) MDR characteristic at 25 and 29. (c) Absolute DVF for different fault types with $R_f = 10\,\Omega$.

on line 26–28. Fig. 8(c) indicates the absolute index values at buses 26 and 28 for different types of fault.

While it is difficult for some of the protection schemes to detect high-impedance faults, it is essential to do so to maintain dependability. An A-G fault is incepted on line 8-9 with different fault resistances (0.1, 1, 50, 100, 200 Ω). To identify the faulty line, first the occurrence of fault is checked for lines 4-5 and 5-6 (SNT-2). Since, the index does not show any fault occurrence till the timer expires, the next step is to check the fault for lines 5–8 and 7-8 using the PMU information at bus-7 and phasor information at bus-5 derived from PMU buses 4 and 6. Again, the timer expires with no result. The last step is to check for a fault on lines 8-9 and 39-9(SNT-1). From Fig. 9(a), for A-G fault of 200 Ω fault resistance, it is observed that the index at 8 and 9 crosses the positive threshold following a fault inception. Since, only bus-8 is the load bus, this condition arises only for fault at line 8-9. Fig. 9(b) shows the effect of the proposed scheme with variations in fault resistances. Although, the magnitude of the index reduces with higher fault resistance, it is still well above the threshold and capable of identifying the faulted line.

The proposed scheme is also tested for different fault locations. A near-end symmetrical fault is created at line 6–11 (SNT-3) at 10% from bus-6. Similarly, a far-end A-G fault at 90% from bus-6 is created. The DVF index at bus-6 crosses the

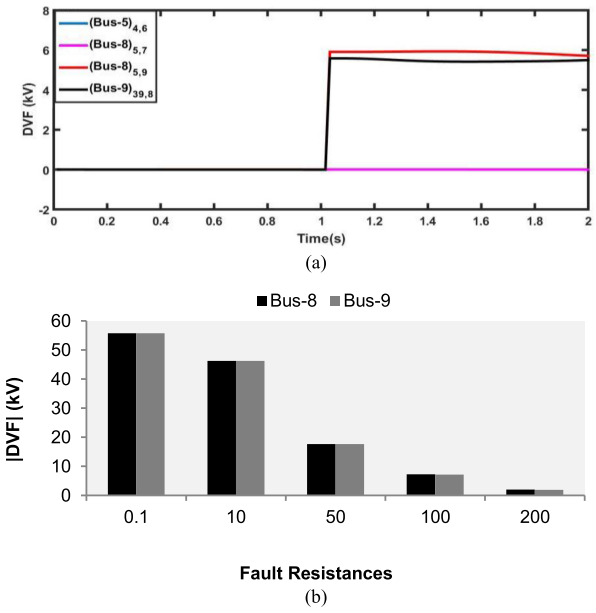


Fig. 9. DVF for (a) A-G fault at line 8-9 with $R_f = 200\,\Omega$ at 1 s and (b) bus-8 and bus-9 for fault at line 8-9 with different fault resistances.

TABLE V
DVF INDEX FOR DIFFERENT FAULTED CONDITIONS

| Faulted Line | Fault type | $R_f$ (Ω) | D (%) | FIA (°) | Affected buses-DVF(kV) | Maximum DVF at non-faulty buses(kV) |
|---|---|---|---|---|---|---|
| 39-9 | ABC | 0.01 | 50 | 0 | 9(39,8),8(7,9)<br>-298,1156 | 0.0026 |
| | AG | 50 | 60 | 30 | -12,44 | -0.0001 |
| | AB | 20 | 40 | 45 | -46,224 | -0.00007 |
| | AB-G | 100 | 20 | 60 | -3,27 | -.0002 |
| 23-24 | ABC | 10 | 50 | 0 | 24(16,23)<br>171 | -0.0012 |
| | AG | 200 | 40 | 90 | 2 | -0.0006 |
| | AB | 50 | 80 | 30 | 7.5 | -0.0006 |
| | AB-G | 100 | 60 | 45 | 6.7 | -0.0005 |
| 10-13 | ABC | 0.1 | 80 | 30 | 13(10,13)<br>15.4 | -0.00105 |
| | B-G | 20 | 20 | 300 | 11.19 | -0.00012 |
| | BC-G | 100 | 50 | 200 | 5.27 | 0.00002 |
| | BC | 50 | 70 | 50 | 4.61 | -0.00038 |
| 4-14 | ABC | 20 | 40 | 0 | 14(4,13)<br>-17.03 | 0.0015 |
| | C-G | 200 | 90 | 90 | -0.17 | 0.0016 |
| | AC-G | 50 | 10 | 45 | -8.64 | 0.0015 |
| | AC | 10 | 60 | 30 | -30.94 | 0.0014 |
| 5-6 | ABC | 0.1 | 10 | 30 | 5(4,6)<br>560 | -0.0012 |
| | A-G | 200 | 90 | 0 | 0.11 | -0.0019 |
| | BC-G | 10 | 40 | 90 | 14.3 | -0.0006 |
| | AC | 50 | 60 | 120 | 1.738 | -0.0003 |

negative threshold for both the cases, as shown in Fig. 10(a)and (b). This verifies a faulted situation at line 6–11. Fig. 10(c) indicates the absolute DVF values at bus-11 for 200 Ω resistance A-G fault with varying fault locations. Table V illustrates the index values for different fault types, fault from resistances ($R_f$), fault inception angles (FIA), and fault location PMU buses or POB.

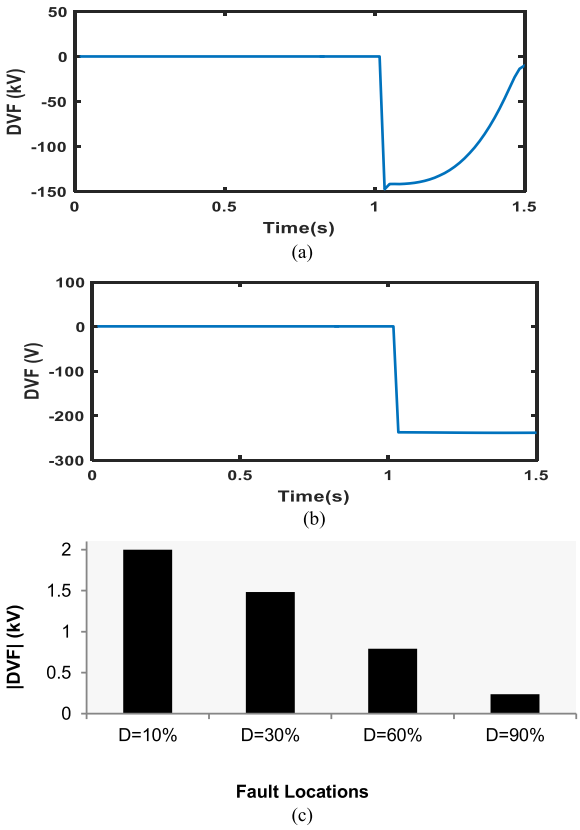


Fig. 10. DVF at bus-11 for (a) bolted symmetrical fault at line 6–11 with $D = 10\%$, (b) L-G fault with $D = 90\%$, and (c) varying fault locations at line 6–11.

From several fault studies, it is observed that the maximum fault detection time for the proposed scheme is about 35 ms. The delays associated with phasor data processing, transducers, and multiplexing may be of the order of 100 ms. Hence, for an independent subnetwork, the response time is 135 ms. A maximum of two subnetworks can be dependent on the phasor information from independent subnetwork, so that the maximum wait time is 200 ms. Hence, for the first and second dependent subnetwork, the response time is around 200 and 300 ms, respectively [32]. Hence, it is within the allowable timer setting range for the backup protection which is around 1000–1800 ms.

### C. Performance Assessment on RTDS

The proposed scheme is executed on RTDS platform (setup shown in Fig. 11) by modeling a modified Western System Coordinating Council (WSCC) 9-bus system (50 Hz frequency) [15] using RSCAD software and loaded onto one of the RTDS racks. It uses PB5 processor for continuous real-time processing at 1.7 GHz with a simulation time step of 50 $\mu$s [33]. Gigabit Transceiver Network card is used to establish connection between RTDS and the system using LAN via Ethernet. The IEEE C37.118.1 compliant GTNET-PMUs utilizing P-class algorithm are embedded inside one of the RTDS racks to fetch the phasor data from the PMU buses 4, 7, and 9 with a reporting rate of 50 frames/s. These are synchronized with GPS clock using GT-SYNC card. The DVF index for three independent subnetworks,

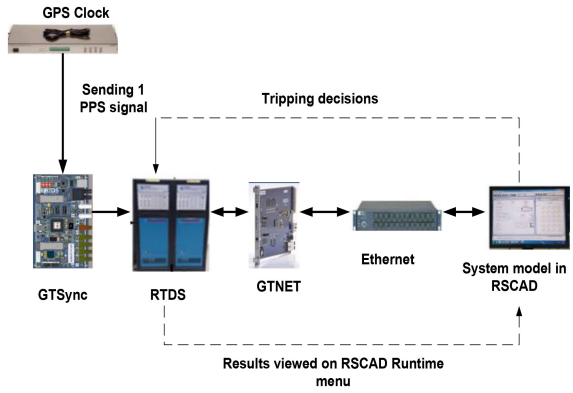


Fig. 11. RTDS setup for the proposed scheme.

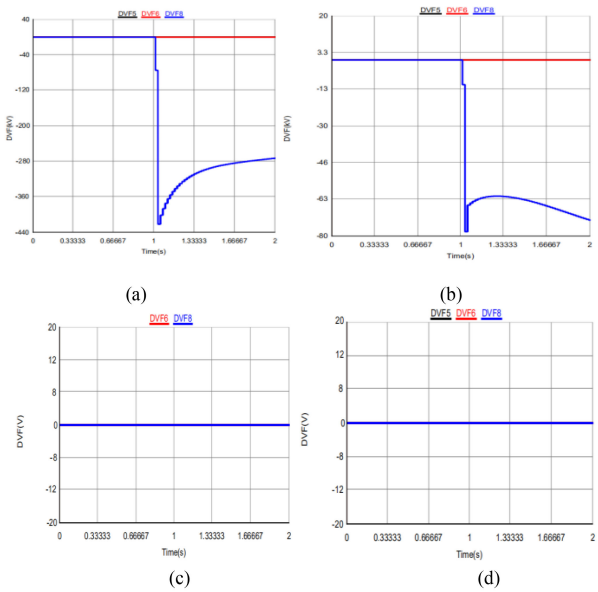


Fig. 12. DVF index for 9-bus system (a) near-end LLL fault, (b) far-end L-G fault, (c) stable power swing for line 7-8, and (d) load increase at bus-8.

i.e., at buses 5 (of 4-5-7), 6 (of 4-6-9), and 8 (of 7-8-9) are calculated. The results are viewed on RSCAD run-time menu.

*Case 1:* A fault at line 7-8 is created at the near end (solid LLL at $D = 10\%$) and far end (L-G for $D = 90\%$ with $R_f = 200\,\Omega$) from bus-7. Fig. 12(a) and (b) shows that the DVF at bus-8 crosses a negative threshold, confirming a fault at line 7-8.

*Case 2:* A fault at line 7–5 is applied at 0.3 s and cleared at 0.4 s to establish a stable swing situation for line 7-8. None of the DVF indexes cross the threshold, as shown in Fig. 12(c), confirming a no-fault situation.

*Case 3:* The load is increased at bus-8 to demonstrate the proposed scheme for load encroachment situation. Fig. 12(d) confirms a no-fault situation, since none of the index values cross the threshold following load increase at 1 s.

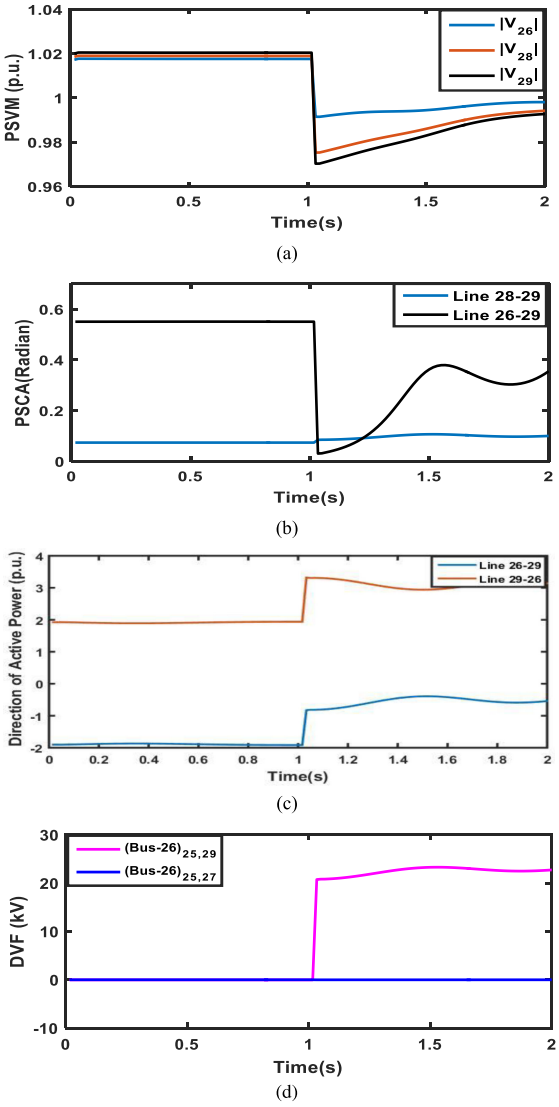


Fig. 13. Comparison of the proposed scheme for L-G fault at line 26–29 near generator bus-29 (a) PSVM, (b) PSCA, (c) DOAP, and (d) DVF at bus-26.

## IV. Comparative Analysis With the Existing Schemes

An L-G fault of 100 Ω resistance is created near the generator at bus-29 at line 26–29. In [7], [9], [17], and [20], it is suggested to find the faulted bus using positive sequence voltage phasors. However, for the present scenario where the fault is very close to the generator bus, the positive sequence voltage magnitudes (PSVM) for the buses closer to the faulted lines are quite similar with minor deviations, as shown in Fig. 13(a). Hence, setting a proper threshold for identifying a faulted bus becomes a difficult task. Even if a minimum voltage criterion is used to identify the faulted bus as bus-26, scheme [7] which uses absolute difference of current angles (PSCA) shows that it does not cross the proposed threshold of 1.74 rad (100°), as shown in Fig. 13(b). This may result if there is no current reversal for internal fault at the line connected to weak source at one terminal while the other terminal is connected to strong source.

Similarly, the direction of active power flow (DOAP) [17] from both the ends of line 26–29 shows an opposite deviation in sign even after the fault case, thus failing to identify the faulted line, as shown in Fig. 13(c). The proposed scheme calculates the DVF index at bus-26 using PMU information at bus-25, 27, and 29. Fig. 13(d) shows that the index crosses the positive threshold for DVF calculated using bus 25 and 29, indicating a fault at line 26–29.

TABLE VI
Performance Limitations of [15]

| Disturbance cases | $\|I_8\|$(p.u.) |
|---|---|
| A-G fault at line 8-9 ($R_f$=50Ω) | 16.309 |
| A-G fault at line 8-9($R_f$=100Ω) | 9.8021 |
| A-G fault at line 8-9($R_f$=200Ω) | 5.3396 |
| Load increase at bus-8 | 5.7621 |

TABLE VII
Comparison With Existing Schemes

| Papers | Fault near strong source/High resistance fault | Stressed conditions | Minimum PMU requirement (39/57 bus) |
|---|---|---|---|
| [7] | - | - | 28/57 |
| [8] | ✓ | - | 9/12 |
| [9] | - | ✓ | 28/57 |
| [10]-[12],[14]-[16], [18], [22] | ✓ | ✓ | 28/57 |
| [13] | ✓ | - | 28/57 |
| [17] | - | ✓ | 28/57 |
| [19] | ✓ | ✓ | 25/35 |
| [20] | ✓ | ✓ | 17/33 |
| [21] | - | ✓ | 13/21 |
| [23] | - | ✓ | >20(39) |
| Proposed | ✓ | ✓ | 14/21 |

In [21], limited PMUs are utilized for FLI where the faulted region is identified using the magnitude of the currents at non-PMU buses derived from PMU buses. However, the usage of prefault load values at the monitored non-PMU buses to find the total current injection at the bus may be unable to distinguish high-resistance fault at connected line and load increase at the bus. To prove this, the magnitude of current injection at bus-8 is calculated from PMUs at buses 6 and 9 (using OPP rules for the scheme). It is observed from Table VI that with increasing fault resistance for fault at 8-9, the current reduces and at 200 Ω, it is less than the value for load increase at bus-8.

Table VII summarizes the comparison of the proposed scheme with other schemes in the literature with respect to minimum PMU requirement, its performance during stressed conditions, and fault near strong source or high-resistance fault.

## V. Conclusion

A WAMs-based differential voltage-based scheme is proposed for FLI in transmission networks. The PMU placement for the proposed scheme ensures fewer PMUs while maintaining system observability. Further, DVF index for each subnetwork is calculated and dependent subnetworks are studied in steps by providing proper timer settings between them. Simulations are carried out in MATLAB/Simulink and RTDS platform to study its effectiveness for several power system disturbances. While

the DVF index for SNT-2 and SNT-3 can directly find the faulted line, for a particular case in SNT-1, there is a requirement of additional schemes to differentiate fault from load increase at the adjacent monitored buses. The proposed scheme is highly secure for different stressed conditions, such as stable power swing, generator outage, load encroachment, and voltage stressed situations. Further, it works effectively for fault situations with various fault types, fault locations, and fault resistances with a maximum response time of 300 ms. The impact of PMU data loss on the backup protection scheme for transmission networks integrated with flexible ac transmission systems (FACTs) and off-shore wind farms is being considered as a future study.

## REFERENCES


[1] P. M. Anderson, *Power System Protection*. New York, NY, USA: McGraw-Hill, 1999.

[2] A. G. Phadke and J. S. Thorp, *Computer Relaying for Power Systems*. New York, NY, USA: Wiley, 2009.

[3] Powergrid, "Report of the enquiry committee on grid disturbance in northern region on 30th July 2012 and in northern, eastern and north-eastern region on 31st July 2012," New Delhi, India, Tech. Rep. GRID_ENQ_REP_16_8_12, 2012.

[4] U.S.-Canada Power System Outage Task Force, "Final report on the August 14, 2003 blackout in the United States and Canada: Causes and recommendations," Rep. no. 20461178, 2004.

[5] M. G. Adamiak *et al.*, "Wide area protection—Technology and infrastructures," *IEEE Trans. Power Del.*, vol. 21, no. 2, pp. 601–609, Apr. 2006.

[6] A. G. Phadke and J. S. Thorp, *Synchronized Phasor Measurements and Their Applications*. New York, NY, USA: Springer, 2008.

[7] M. M. Eissa, M. E. Masoud, and M. M. M. Elanwar, "A novel back up wide area protection technique for power transmission grids using phasor measurement unit," *IEEE Trans. Power Del.*, vol. 25, no. 1, pp. 270–278, Jan. 2010.

[8] M. K. Neyestanaki and A. M. Ranjbar, "An adaptive PMU-based wide area backup protection scheme for power transmission lines," *IEEE Trans. Smart Grid*, vol. 6, no. 3, pp. 1550–1559, May 2015.

[9] P. K. Nayak, A. K. Pradhan, and P. Bajpai, "Wide-area measurement-based backup protection for power network with series compensation, *IEEE Trans. Power Del.*, vol. 29, no. 4, pp. 1970–1977, Aug. 2014.

[10] Z. He, Z. Zhang, W. Chen, O. P. Malik, and X. Yin, "Wide-area backup protection algorithm based on fault component voltage distribution," *IEEE Trans. Power Del.*, vol. 26, no. 4, pp. 2752–2760, Oct. 2011.

[11] A. Dwivedi, B. Mallikarjuna, D. Pal, M. J. B. Reddy, and D. K. Mohanta, "A real-time synchrophasor-based zone-3 supervision of distance relays under load encroachment condition," *IEEE Syst. J.*, vol. 13, no. 4, pp. 4227–4235, Dec. 2019.

[12] Z. Lia, Y. Wana, L. Wub, Y. Chenga, and H. Weng, "Study on wide-area protection algorithm based on composite impedance directional principle," *Int. J. Elect. Power Energy Syst.*, vol. 115, pp. 105–118, 2020.

[13] T. G. Bolandi, H. Seyedi, S. M. Hashemi, and P. S. Nezhad, "Impedance-differential protection: A new approach to transmission-line pilot protection," *IEEE Trans. Power Del.*, vol. 30, no. 6, pp. 2510–2518, Dec. 2015.

[14] T. P. Hinge and S. S. Dambhare, "Secure phase comparison schemes for transmission-line protection using synchrophasors," *IEEE Trans. Power Del.*, vol. 30, no. 4, pp. 2045–2054, Aug. 2015.

[15] M. K. Jena, S. R. Samantaray, and B. K. Panigrahi, "A new wide-area backup protection scheme for series-compensated transmission system," *IEEE Syst. J.*, vol. 11, no. 3, pp. 1877–1887, Sep. 2017.

[16] S. Das and B. K. Panigrahi, "Real-time secured third zone relay operation under dynamic stressed conditions," *IEEE Syst. J.*, vol. 13, no. 3, pp. 3337–3346, Sep. 2019.

[17] V. Nougain, M. K. Jena, and B. K. Panigrahi, "Synchro-phasors assisted back-up protection of transmission line," *IET Gener., Transmiss. Distrib.*, vol. 12, no. 14, pp. 3414–3420, Aug. 2018.

[18] V. Nougain, M. K. Jena, and B. K. Panigrahi, "Decentralised wide-area back-up protection scheme based on the concept of centre of reactive power," *IET Gener., Transmiss. Distrib.*, vol. 13, no. 20, pp. 4551–4557, 2019.

[19] J. Zare, F. Aminifar, and M. Sanaye-Pasand, "Synchrophasor-based wide-area backup protection scheme with data requirement analysis," *IEEE Trans. Power Del.*, vol. 30, no. 3, pp. 1410–1419, Jun. 2015.

[20] B. K. S. Roy, R. Sharma, A. K. Pradhan, and A. K. Sinha, "Faulty line identification algorithm for secured backup protection using PMUs," *Elect. Power Compon. Syst.*, vol. 45, no. 5, pp. 491–504, 2017.

[21] A. Sharafi, M. Sanaye-Pasand, and F. Aminifar, "Transmission system wide-area back-up protection using current phasor measurements," *Int. J. Elect. Power Energy Syst.*, vol. 92, pp. 93–103, 2017.

[22] P. Kundu and A. K. Pradhan, "Power network protection using wide-area measurements considering uncertainty in data availability," *IEEE Syst. J.*, vol. 12, no. 4, pp. 3358–3368, Dec. 2018.

[23] M. K. Jena, S. R. Samantaray, and B. K. Panigrahi, "A new decentralized approach to wide-area back-up protection of transmission lines," *IEEE Syst. J.*, vol. 12, no. 4, pp. 3161–3168, Dec. 2018.

[24] B. Mallick and S. Chakrabarti, "Optimal placement of phasor measurement units for multi-area observability," in *Proc. ISGT2011-India*, Kollam, Kerala, 2011, pp. 12–16.

[25] M. A. Pai, *Energy Function Analysis for Power System Stability*. Norwell, MA, USA: Kluwer, 1989.

[26] I. Kamwa, S. R. Samantaray, and G. Joos, "Compliance analysis of PMU algorithms and devices for wide-area stabilizing control of large power systems," *IEEE Trans. Power Syst.*, vol. 28, no. 2, pp. 1766–1778, May 2013.

[27] I. Kamwa, S. R. Samantaray, and G. Joos, "Wide frequency range adaptive phasor and frequency PMU algorithms," *IEEE Trans. Smart Grid*, vol. 5, no. 2, pp. 569–579, Mar. 2014.

[28] *IEEE Standard for Synchrophasor Measurements for Power Systems*, IEEE Standard C37.118.1-2011 (Revision of IEEE Standard C37.118, 2005.

[29] *IEEE Standard for Synchrophasor Measurements for Power Systems – Amendment 1: Modification of Selected Performance Requirements*, IEEE Std C37.118.1a-2014 (Amendment to IEEE Standard C37.118.1-2011), Apr. 30 2014.

[30] IEEE Power System Relaying Committee of the IEEE Power Eng. Soc., "Power swing and out-of-step consideration on transmission lines," Rep. PSRC WG D6, Jul. 2005. [Online]. Available: http://www.pes-psrc.org

[31] NERC, "Relay loadability exceptions: Determination and application of practical relaying loadability ratings," Aug. 2005. [Online]. Available: http://www.nerc.com/∼filez/spctf.html

[32] B. Naduvathuparambil, M. C. Valenti, and A. Feliachi, *Of Communication Delays in Wide Area Measurement Systems Lane*. Morgantown, WV, USA: Dept. Comp. Sci. Elect. Eng., West Virginia Univ., 2002, pp. 26506–26109.

[33] *Real Time Digital Simulator Power System Users Manual RTDS Technologies*, Winnipeg, MB, Canada, 2006.


**Shalini** received the master's degree in power systems from the Birla Institute of Technology Mesra, Ranchi, India, in 2015. She is currently working toward the Ph.D. degree with the School of Electrical Sciences, Indian Institute of Technology Bhubaneswar, Bhubaneswar, India.

Her research interests include wide-area backup protection.

**Subhransu Ranjan Samantaray** (Senior Member, IEEE) received the B.Tech. degree from UCE Burla, Burla, India, and the Ph.D. degree from the National Institute of Technology Rourkela, Rourkela, India.

He was a Postdoctoral Researcher with McGill University, Montreal, QC, Canada. He is currently an Associate Professor with the School of Electrical Sciences, Indian Institute of Technology Bhubaneswar, Bhubaneswar, India. His major research interests include PMU and wide-area measurement, intelligent protection for transmission systems including FACTs, microgrid protection including distributed generation, microgrid planning, wide-area-based dynamic security assessment in large power networks and smart-grid technologies.

Dr. Samantaray is a Fellow of the Institution of Engineering and Technology (IET), U.K. and a Member of the IEEE Power Systems Stability Subcommittee. He was the recipient of the prestigious NASI-SCOPUS Young Scientists Award 2015, IEEE Power and Energy Society Technical Committee Prize Paper Award 2012, Samanta Chandra Sekhar Award, Odisha Bigyana Academy 2010, etc. He is an Associate Editor for the IEEE SYSTEMS JOURNAL, IEEE TRANSACTIONS ON SMART GRID, a former Associate Editor for the IEEE TRANSACTIONS ON POWER DELIVERY, *IET Generation, Transmission and Distribution*, and a Guest Editor for the IEEE SENSORS JOURNAL.